Comput Visual Sci 6: 67–74 (2004)
Digital Object Identifier (DOI) 10.1007/s00791-003-0110-3

Computing and
Visualization in Science

Regular article

Mathematical model and numerical simulation of the liquid fluidization of polydisperse solid particle mixtures

S. Berres[1], **R. Bürger**[1], **E.M. Tory**[2]

[1] Institut für Angewandte Analysis und numerische Simulation, Universität Stuttgart, Pfaffenwaldring 57, D-70569 Stuttgart, Germany
(e-mail: {berres, buerger}@mathematik.uni-stuttgart.de)
[2] Professor Emeritus, Department of Mathematics and Computer Science, Mount Allison University, Sackville, NB, E4L 1E8, Canada
(e-mail: sherpa@nbnet.nb.ca)

Received: 20 July 2002 / Accepted: 23 March 2003
Published online: 23 January 2004 – © Springer-Verlag 2004

Communicated by: M.S. Espedal, A. Quarteroni, A. Sequeira

Abstract. A mathematical model for the fluidization of polydisperse suspensions is developed. The stationary concentration configurations for a given fluidizing velocity are analyzed and a mixing condition for bed inversion is derived. A central finite difference scheme is applied to the simulation of the fluidization of a bidisperse suspension. The numerical simulations agree with the experimentally reported qualitative behaviour of fluidized suspensions such as bed expansion and bed inversion.

1 Introduction

Mathematical models of polydisperse suspensions consisting of small solid particles of N species that may differ in density or size are important in numerous applications in chemical engineering, wastewater treatment and medicine. In one space dimension and if sediment compressibility effects are neglected, model equations for such mixtures reduce to a strongly coupled system of first-order conservation laws. In a series of papers, the type behaviour of these one-dimensional (not necessarily hyperbolic) model equations was analyzed [1, 5], and the equations were solved numerically by high-resolution central difference schemes [14, 19] in order to simulate the differential settling of polydisperse suspensions in batch columns [2, 4]. These schemes generally turned out to be useful for exploring the settling dynamics of polydisperse systems and have meanwhile been adopted by other groups for the same purpose [23].

On the other hand, the same one-dimensional model equations can be utilized to describe fluidization processes, in which a relatively compact layer of solid particles (usually called a 'bed') is resuspended ('fluidized') by an applied upwards (counter-gravity) bulk flow of fluid. This process is important in applications and gives rise to fascinating phenomena, especially when particles of different sizes and densities are involved. These include layer inversion and complete mixing, which have received considerable attention in the chemical engineering literature (see e.g. [11–13, 17, 18, 20]). However, to our knowledge, all studies have been concerned with fluidization *experiments* and with the derivation of criteria for the occurence of complete mixing or layer inversion. It is the purpose of the present contribution to complement these findings by showing that *simulations* with modern shock-capturing schemes can be employed to examine the dynamics of these fluidization processes and thereby to validate model equations. To put this observation (and the present paper) in the proper perspective, we mention that all conventional analyses have been concerned with conditions for the existence and characterization of *steady* fluidized states, while we demonstrate that these states are *produced* (in some sense, appear 'automatically') by solving the nonlinear conservation equations with an appropriate composition of the initial mixture and applied flow velocities. Thus, the present paper combines mathematical modelling and numerical simulations to draw attention to a seldom considered application of systems of conservation laws.

It should be mentioned that, for arbitrary N, an existence and uniqueness theory for the polydisperse sedimentation and fluidization model, which forms a special case of strongly coupled first-order systems of conservation laws, is not yet available. In fact, a counter-gravity bulk velocity (as needed to fluidize a bed of particles of a density larger than that of the fluid) is explicitly excluded from the uniqueness analysis of scalar convection-diffusion equations [3, 6], which up to the sign of this bulk velocity include the case $N = 1$ of the fluidization model presented herein.

This paper is organized as follows. Section 2 provides a brief derivation of the Masliyah-Lockett-Bassoon (MLB) model [15, 16] of polydisperse suspensions, which leads to a system of first-order conservation laws. Recently established basic properties of these equations are recalled. A criterion for layer inversion according to the MLB model is derived in Sect. 3. In Sect. 4 the numerical method is briefly recalled and adapted. Numerical simulations are shown in Sect. 5. A discussion of our results is provided in Sect. 6.

2 Mathematical model

In this section, we briefly derive the equations describing sedimentation and fluidization of polydisperse suspensions of

rigid spheres. For additional details and justifications, we refer to [1, 5]. Unless otherwise stated, the index i counting the particle species runs from 1 to N.

The local mass balance equations of the solid species and of the fluid can be written as

$$\frac{\partial \phi_i}{\partial t} + \nabla \cdot \left(\phi_i \boldsymbol{v}_i\right) = 0\,, \tag{1}$$

$$-\frac{\partial \phi}{\partial t} + \nabla \cdot \left((1-\phi)\boldsymbol{v}_\mathrm{f}\right) = 0\,, \tag{2}$$

where $\phi := \phi_1 + \cdots + \phi_N$ is the total solids volume fraction and $\boldsymbol{v}_i$, $\boldsymbol{v}_\mathrm{f}$ are the solids and fluid velocities, respectively. Defining the volume-average velocity of the mixture $\boldsymbol{q} := (1-\phi)\boldsymbol{v}_\mathrm{f} + \phi_1 \boldsymbol{v}_1 + \cdots + \phi_N \boldsymbol{v}_N$ and the slip or relative velocities $\boldsymbol{u}_i := \boldsymbol{v}_i - \boldsymbol{v}_\mathrm{f}$, we obtain

$$\phi_i \boldsymbol{v}_i = \phi_i \left(\boldsymbol{u}_i + \boldsymbol{q} - \sum_{m=1}^{N} \phi_m \boldsymbol{u}_m \right); \tag{3}$$

hence the mass balance equations (1) can be rewritten in terms of $\boldsymbol{q}$ and $\boldsymbol{u}_1, \ldots, \boldsymbol{u}_N$ as

$$\frac{\partial \phi_i}{\partial t} + \nabla \cdot \left(\phi_i \boldsymbol{u}_i + \phi_i \boldsymbol{q} - \phi_i \sum_{m=1}^{N} \phi_m \boldsymbol{u}_m \right) = 0\,. \tag{4}$$

The sum of all equations (1) and equation (2) produces the simple mass balance of the mixture

$$\nabla \cdot \boldsymbol{q} = 0\,. \tag{5}$$

The momentum-balance equations are

$$\varrho_i \phi_i \frac{\mathrm{D}\boldsymbol{v}_i}{\mathrm{D}t} = \nabla \cdot \boldsymbol{T}_i + \varrho_i \phi_i \boldsymbol{b} + \boldsymbol{m}_i^\mathrm{f} + \sum_{k=1}^{N} \boldsymbol{m}_{ik}^\mathrm{s}\,, \tag{6}$$

$$\varrho_\mathrm{f} (1-\phi) \frac{\mathrm{D}\boldsymbol{v}_\mathrm{f}}{\mathrm{D}t} = \nabla \cdot \boldsymbol{T}_\mathrm{f} + \varrho_\mathrm{f} (1-\phi)\boldsymbol{b} - \sum_{i=1}^{N} \boldsymbol{m}_i^\mathrm{f}\,. \tag{7}$$

Here, ϱ_i and ϱ_f denote the densities of the solids and the fluid, respectively, $\boldsymbol{T}_i$ denotes the stress tensor of particle species i, $\boldsymbol{T}_\mathrm{f}$ that of the fluid, $\boldsymbol{b}$ is the body force, $\boldsymbol{m}_i^\mathrm{f}$ and $\boldsymbol{m}_{ij}^\mathrm{s}$ are the interaction forces per unit volume between solid species i and the fluid and between the solid species i and j, respectively, and we use the standard notation $\mathrm{D}\boldsymbol{v}/\mathrm{D}t := \partial \boldsymbol{v}/\partial t + (\boldsymbol{v} \cdot \nabla)\boldsymbol{v}$.

It is assumed that the only body force is gravity, $\boldsymbol{b} = -g\boldsymbol{k}$, where g is the acceleration of gravity and $\boldsymbol{k}$ is the upwards-pointing unit vector.

We assume that the stress tensors of the solid and fluid phases can be written as $\boldsymbol{T}_i = -p_i \boldsymbol{I} + \boldsymbol{T}_i^\mathrm{E}$ and $\boldsymbol{T}_\mathrm{f} = -p_\mathrm{f} \boldsymbol{I} + \boldsymbol{T}_\mathrm{f}^\mathrm{E}$, respectively, where p_i denotes the phase pressure of particle species i, p_f that of the fluid, $\boldsymbol{I}$ denotes the identity tensor, and $\boldsymbol{T}_i^\mathrm{E}$ and $\boldsymbol{T}_\mathrm{f}^\mathrm{E}$ are the extra (or viscous) stress tensors of particle species i and the fluid, respectively, all of which could be given by expressions that correspond to a viscous-linear fluid. Since the focus here is on the continuity equations for the solid species, and we assume that viscous effects due to the motion of the mixture are not dominant, all viscous effects are assigned to the fluid extra-stress tensor.

The pressures p_i and p_f are theoretical variables that cannot be measured experimentally. For monodisperse suspensions forming compressible sediments [7, 8], these variables are expressed in terms of the pore pressure p and the effective solid stress σ_e. However, since the particles are rigid incompressible spheres, we assume $\sigma_\mathrm{e} \equiv 0$. As in [1, 5], we relate the phase pressures p_i to the total pressure $p_\mathrm{t} := p_1 + \cdots + p_N + p_\mathrm{f} = p + \sigma_\mathrm{e}$ by $p_i = \phi_i p_\mathrm{t}$.

Furthermore, for a monodisperse suspension, the interaction force $\boldsymbol{m}$ between the fluid and the unique solid phase can be modeled by $\boldsymbol{m} = \alpha(\phi)\boldsymbol{u} + \beta \nabla \phi$, where α is the resistance coefficient, $\boldsymbol{u} := \boldsymbol{v}_\mathrm{s} - \boldsymbol{v}_\mathrm{f}$ is the solid-fluid relative velocity (or slip velocity), and the coefficient β coincides with the pore pressure p [7]. In the present case, we analogously assume that the solid-fluid interaction term $\boldsymbol{m}_i^\mathrm{f}$ corresponding to species i is given by $\boldsymbol{m}_i^\mathrm{f} = \alpha_i(\Phi)\boldsymbol{u}_i + \beta \nabla \phi_i$, where α_i denotes the resistance coefficient related to the transfer of momentum between the fluid and solid phase species i.

The interaction force between the different solid particle species could be specified by a formula like that of Nakamura and Capes (stated explicitly in [1, 5]), but there is considerable experimental and theoretical evidence [5] that these interaction forces can be neglected at the very low Reynolds numbers considered here.

Inserting the present constitutive assumptions into (6) and (7) and considering the mixture at equilibrium ($t \to \infty$) in a settling column, i.e. when $\boldsymbol{v}_\mathrm{f} = 0$, $\boldsymbol{u}_1 = \cdots = \boldsymbol{u}_N = 0$ and $\nabla p = -\varrho_\mathrm{f} g \boldsymbol{k}$, we obtain $\beta = p$ [5, 7]. The linear momentum-balances now are

$$\varrho_i \phi_i \frac{\mathrm{D}\boldsymbol{v}_i}{\mathrm{D}t} = -\varrho_i \phi_i g \boldsymbol{k} + \nabla \cdot \boldsymbol{T}_i^\mathrm{E} - \phi_i \nabla p + \alpha_i(\Phi)\boldsymbol{u}_i + \boldsymbol{m}_i^\mathrm{s}\,, \tag{8}$$

$$\begin{aligned} \nabla p = &-\varrho_\mathrm{f} g \boldsymbol{k} - \frac{1}{1-\phi} \sum_{m=1}^{N} \alpha_m(\Phi)\boldsymbol{u}_m \\ &- \varrho_\mathrm{f} \frac{\mathrm{D}\boldsymbol{v}_\mathrm{f}}{\mathrm{D}t} + \frac{1}{1-\phi} \nabla \cdot \boldsymbol{T}_\mathrm{f}^\mathrm{E}\,. \end{aligned} \tag{9}$$

After a dimensional analysis [1, 5] and assuming the typical parameter values $d = 10^{-4}\,\mathrm{m}$ (size of the largest particles), $g = 10\,\mathrm{m/s^2}$ (acceleration of gravity), $L = 1\,\mathrm{m}$ (height of a settling vessel), $U = 10^{-4}\,\mathrm{m/s}$ (settling velocity of a particle of the fastest species in an unbounded fluid) and $\nu_0^\mathrm{f} = 10^{-6}\,\mathrm{m^2/s}$, we discard the advective acceleration and viscous terms from (8) and the advective acceleration term from (9) (but we here retain the viscous term), which leads to the following simplified linear momentum balances:

$$\alpha_i(\Phi)\boldsymbol{u}_i = \varrho_i \phi_i g \boldsymbol{k} + \phi_i \nabla p\,, \tag{10}$$

$$\nabla p = -\varrho_\mathrm{f} g \boldsymbol{k} - \frac{1}{1-\phi} \sum_{m=1}^{N} \alpha_m(\Phi)\boldsymbol{u}_m + \frac{1}{1-\phi} \nabla \cdot \boldsymbol{T}_\mathrm{f}^\mathrm{E}\,. \tag{11}$$

Inserting (11) into (10), we obtain

$$\begin{aligned} &\frac{\alpha_i(\Phi)(1-\phi)}{\phi_i}\boldsymbol{u}_i + \sum_{i=1}^{N} \alpha_i(\Phi)\boldsymbol{u}_i = \boldsymbol{r}_i\,, \\ &\boldsymbol{r}_i := (1-\phi)\left((\varrho_i - \varrho_\mathrm{f})\, g\boldsymbol{k}\right) + \nabla \cdot \boldsymbol{T}_\mathrm{f}^\mathrm{E}\,. \end{aligned} \tag{12}$$

The linear system (12) for the unknowns $\boldsymbol{u}_1, \ldots, \boldsymbol{u}_N$ can be solved explicitly by the Sherman-Morrison formula [5]. The solution is

$$\boldsymbol{u}_i = \frac{\phi_i}{\alpha_i(\Phi)(1-\phi)} \left(\boldsymbol{r}_i - (\phi_1 \boldsymbol{r}_1 + \cdots + \phi_N \boldsymbol{r}_N) \right). \tag{13}$$

Let $\varrho(\Phi) := (1-\phi)\varrho_\mathrm{f} + \phi_1\varrho_1 + \cdots + \phi_N\varrho_N$ denote the local density of the mixture and note that $\phi_1(\varrho_1 - \varrho_\mathrm{f}) + \cdots + \phi_N(\varrho_N - \varrho_\mathrm{f}) = \varrho(\Phi) - \varrho_\mathrm{f}$. Inserting $\boldsymbol{r}_1, \ldots, \boldsymbol{r}_N$ into (13) and neglecting the viscous term $\nabla \cdot \boldsymbol{T}_\mathrm{f}^\mathrm{E}$ leads to an explicit equation for the slip velocities $\boldsymbol{u}_i$ as functions of Φ, which after rearranging reads

$$\boldsymbol{u}_i = \frac{\phi_i}{\alpha_i(\Phi)}\big(\varrho_i - \varrho(\Phi)\big)g\boldsymbol{k}\,. \tag{14}$$

The specific assumption of the MLB model is the equation

$$\frac{\phi_i}{\alpha_i(\Phi)} = -\frac{d_i^2 V(\phi)}{18\mu_\mathrm{f}}\,, \tag{15}$$

where μ_f is the viscosity of the pure fluid, and the hindered settling factor $V(\phi)$ could, for example, be chosen as $V(\phi) = (1-\phi)^{n-2}$.

It is convenient to introduce the reduced densities $\bar{\varrho}_\mathrm{s} := \varrho_\mathrm{s} - \varrho_\mathrm{f}$, $\bar{\varrho}_i := \varrho_i - \varrho_\mathrm{f}$, the vector $\bar{\boldsymbol{\varrho}} := (\bar{\varrho}_1, \ldots, \bar{\varrho}_N)^\mathrm{T}$, and the parameters $\mu := -gd_1^2/(18\mu_\mathrm{f})$ and $\delta_i := d_i^2/d_1^2$, so that the final expression for the slip velocities reads

$$\boldsymbol{u}_i = \mu\delta_i\left(\bar{\varrho}_i - \bar{\boldsymbol{\varrho}}^\mathrm{T}\Phi\right)V(\Phi)\boldsymbol{k}\,. \tag{16}$$

The final model equations are the continuity equations of the solids species (1) and of the mixture (5), the linear momentum balance of the fluid (11), and the equations (16) for the slip velocities $\boldsymbol{u}_i$, which have been obtained from the linear-momentum balances of the solid species. Inserting (16) into (1) and (11), we obtain the final system of model equations:

$$\frac{\partial\phi_i}{\partial t} + \nabla\cdot\big(\phi_i\boldsymbol{q} + f_i(\Phi)\boldsymbol{k}\big) = 0\,, \tag{17}$$

$$\nabla\cdot\boldsymbol{q} = 0\,, \tag{18}$$

$$\nabla p = -\varrho(\Phi)g\boldsymbol{k} + \frac{1}{1-\phi}\nabla\cdot\boldsymbol{T}_\mathrm{f}^\mathrm{E}\,. \tag{19}$$

Specifically for the MLB model, the components of the flux density vector $\boldsymbol{f}(\Phi)$ are given by

$$f_i(\Phi) = f_i^\mathrm{M}(\Phi) = \mu V(\Phi)\phi_i\Big[\delta_i\left(\bar{\varrho}_i - \bar{\boldsymbol{\varrho}}^\mathrm{T}\Phi\right) - \big(\delta_1\phi_1\left(\bar{\varrho}_1 - \bar{\boldsymbol{\varrho}}^\mathrm{T}\Phi\right) + \cdots + \delta_N\phi_N\left(\bar{\varrho}_N - \bar{\boldsymbol{\varrho}}^\mathrm{T}\Phi\right)\big)\Big]\,. \tag{20}$$

The viscous effects expressed by (19) are relevant in several space dimensions only [1, 5]. For the application considered in this paper, the discussion can be limited to one space dimension. In this case, we get $\partial q/\partial z = 0$, and only (17) needs to be solved, since q is given by boundary conditions and (19) turns into an equation for the pore pressure p, which permits us to calculate this quantity a posteriori from the concentrations $\phi_1, \ldots, \phi_N$. Thus, the system of interest is

$$\frac{\partial\phi_i}{\partial t} + \frac{\partial}{\partial x}\big(q(t)\phi_i + f_i^\mathrm{M}(\Phi)\big) = 0\,. \tag{21}$$

We consider (21) in a vertical fluidization column of (normalized) height one, i.e. $0 \le x \le 1$. At the bottom end $x = 0$, clear liquid is fed into the column, and we may assume that at $x = 1$ a sieve is provided to retain the fluidized particles in the unit. This corresponds to the kinematic boundary conditions

$$q(t)\phi_i(x_\mathrm{b}, t) + f_i^\mathrm{M}\big(\Phi(x_\mathrm{b}, t)\big) = 0, \quad x_\mathrm{b} \in \{0, 1\}\,. \tag{22}$$

It was recently proved [1] that, in the equal-density case ($\varrho_1 = \cdots = \varrho_N = \varrho_\mathrm{s}$) and for arbitrary numbers N and particle size distributions, the system (21) (with the flux vector (20)) is strictly hyperbolic (i.e., the Jacobian $\mathcal{J}_{f^\mathrm{M}}(\Phi)$ has N distinct eigenvalues) in the interior of the domain of physically relevant concentrations

$$\mathcal{D}_{\phi_\mathrm{max}} := \big\{\Phi \in \mathbb{R}^N : \phi_1 \ge 0, \ldots, \phi_N \ge 0,\ \phi \le \phi_\mathrm{max}\big\},$$

where $0 < \phi_\mathrm{max} \le 1$ is a maximum concentration at which $V(\phi)$ is cut. This property of the MLB model contrasts, for example, with Davis and Gecol's model equations [9], which for $N = 2$ are hyperbolic for small values of d_1/d_2 (typically, $d_1/d_2 \le 5$) only [5].

On the other hand, it was shown in [5] that the equations (20), (21) are in general not hyperbolic for suspensions in which two or more species have different densities. In particular, for $N = 2$ they are of mixed hyperbolic-elliptic type. The degeneracy into non-hyperbolic type is a criterion for the possible occurrence of horizontal structures like vertical fingers, columns or blobs during sedimentation. These instability phenomena are particularly likely to occur in polydisperse suspensions including one species that is heavier and one that is lighter than the fluid [22]. The precise shape of the instability region as a subset of $\mathcal{D}_{\phi_\mathrm{max}}$ usually has to be determined numerically. However, for bidisperse suspensions of equal-sized spheres in which both particle species are heavier than the fluid ($\varrho_1, \varrho_2 > \varrho_\mathrm{f}$) and the solid densities differ only slightly ($\varrho_1 \approx \varrho_2$), the instability (ellipticity) region in the interior of $\mathcal{D}_1$ is small and located near the line $\phi_1 + \phi_2 = 1$, such that cutting $V(\phi)$ appropriately again produces a hyperbolic model [5].

3 Mixing condition for bed inversion

In fluidization of polydisperse mixtures, bed expansion and bed inversion are the two most interesting phenomena, whose description forms a major challenge to both experiments and models [10, 11]. The principal parameter of interest in bed expansion is the height of the mixture, whereas for bed inversion it is the qualitative composition of the suspension, each time as a function of the applied fluidization velocity. One of the interesting questions in bed inversion is that of the appropriate fluidization velocity that leads to a stable, completely mixed fluidized bed.

Moritomi et al. [18] provide a vivid description of the bed inversion phenomenon: "*When a mixture of a given amount of lighter and heavier particles is fluidized at low liquid velocities, the bed is almost completely segregated; most of the lighter particles segregate to the upper part of the bed, leaving only a small amount of them in the lower heavier-particle-rich layer. The population of the lighter particles in the lower layer increases gradually with the velocity, and at a certain velocity both particles mix completely. A further increase of the velocity then results in a drastic change of the mixing state. The bed again stratifies into two layers but with inverse order of the layers, i.e. the heavier-particle-rich layer in the upper part of the bed and the lighter-particle-rich layer in the lower part.*"

We now derive the conditions under which the solution of the transient MLB model equation may produce a completely

mixed fluidized bed. More precisely, we consider polydisperse suspensions with solid particles of N species differing in size and density, and are interested in determining the concentration ϕ_i^* of each species such that a completely mixed state exists at which the particles remain at fixed positions despite a positive applied bulk flow velocity q. The calculation can be performed without taking into account the value of q. In fact, the assumption that the particles stay at fixed positions can be expressed as

$$F_i\left(\Phi^*\right) := \phi_i^* v_i = \phi_i^* q + \phi_i^* u_i - \phi_i^* \sum_{m=1}^{N} \phi_m^* u_m = 0\,. \tag{23}$$

Inserting the definition of the slip velocities (16) and noting that we may assume $\phi_i^* > 0$ for all $i = 1, \ldots, N$, since we could otherwise reduce the disussion to a mixed state for a smaller number of species, we see that (23) is a nonlinear system of N equations, where one single equation can be written in the form

$$\left(\Phi^*\right)^{\mathrm{T}} \boldsymbol{A}\Phi^* + \boldsymbol{b}_i\Phi^* + \bar{\varrho}_i\delta_i + \frac{q}{\mu V\left(\Phi^*\right)} = 0\,, \tag{24}$$

where $\boldsymbol{A} := \boldsymbol{\delta}\bar{\boldsymbol{\varrho}}^{\mathrm{T}}$ and $\boldsymbol{b}_i := -(\delta_1\varrho_1, \ldots, \delta_N\varrho_N) - \delta_i\bar{\boldsymbol{\varrho}}^{\mathrm{T}}$. Observe that, in the stationary state, $F_i\left(\Phi^*\right) = F_j\left(\Phi^*\right)$ for $i, j = 1, \ldots, N$. Thus equating the left-hand parts of (24) for i and $j, i \neq j$, leads to the equations

$$\bar{\boldsymbol{\varrho}}^{\mathrm{T}}\Phi^* = \frac{\bar{\varrho}_j\delta_j - \bar{\varrho}_i\delta_i}{\delta_j - \delta_i}, \quad 1 \leq i \neq j \leq N\,. \tag{25}$$

Observe that (25) is a rank one linear system of $N-1$ independent equations in N variables. For $N = 2$, the case we exclusively consider in this paper, (25) describes the line

$$\phi_2^* = -\frac{\bar{\varrho}_1}{\bar{\varrho}_2}\phi_1^* + \frac{\bar{\varrho}_2\delta_2 - \bar{\varrho}_1\delta_1}{(\delta_2 - \delta_1)\bar{\varrho}_2} \tag{26}$$

in phase space. For $N > 2$, (25) describes analogously an $(N-1)$-dimensional hyperplane in the phase space provided that the parameters δ_i and $\bar{\varrho}_i$ appearing on the right-hand part satisfy a compatibility condition, which requires that for different index pairs (i, j) and (k, l), the right hand side of (26) is unique. For arbitrarily prescribed particle properties, the compatibility condition is violated. Thus, the system (25) might not be solvable at all and, in that case, a complete mixing is not feasible.

Next, we assume that a vector $\Phi^* := (\phi_1^*, \phi_2^*)^{\mathrm{T}}$ satisfying (25) (corresponding to a desired composition of a completely mixed state) has been chosen. The corresponding fluidization velocity is then given by

$$q^* = -\left(1 - \phi^*\right)\mu V\left(\Phi^*\right)\left(\bar{\varrho}_1 - \bar{\boldsymbol{\varrho}}^{\mathrm{T}}\Phi^*\right). \tag{27}$$

Finally, to attain the completely mixed state by numerical solution of the time-dependent model equations, we have to choose the initial data according to the desired mixed state. If we restrict ourselves to suspensions with constant initial concentrations, then the condition

$$\frac{\phi_2^*}{\phi_1^*} = \frac{\phi_2^0}{\phi_1^0} \tag{28}$$

must be satisfied.

In the numerical example, we consider $N = 2$ and the parameters $d_1 = 1.5 \times 10^{-4}\,\mathrm{m}$, $d_2 = 3.0 \times 10^{-5}\,\mathrm{m}$, $\varrho_1 = 1500\,\mathrm{kg/m^3}$, $\varrho_2 = 2500\,\mathrm{kg/m^3}$ and a fluid density $\varrho_{\mathrm{f}} = 1000\,\mathrm{kg/m^3}$, such that $\boldsymbol{\delta} = (1, 0.04)^{\mathrm{T}}$ and $\bar{\boldsymbol{\varrho}} = (500, 1500)^{\mathrm{T}}\,\mathrm{kg/m^3}$. The masses of individual spherical particles of Species 1 and 2 are $m_1 = 2.65\,\mathrm{mg}$ and $m_2 = 0.035\,\mathrm{mg}$, respectively, so that the larger particles are also the heavier particles. (Note, however, that the larger particles are less dense.) For these parameters, (26) corresponds to the straight line joining all possible mixed states (ϕ_1^*, ϕ_2^*) drawn in Fig. 1.

Moreover, we assume $g = 9.81\,\mathrm{m/s^2}$, the fluid viscosity $\mu_{\mathrm{f}} = 10^{-3}\,\mathrm{Pa\cdot s}$ and the hindered settling function $V(\Phi) = V(\phi) = (1-\phi)^{n-2}$ with $n = 4.7$. These values imply $\mu = -1.23 \times 10^{-5}\,\mathrm{m^4/(kg\cdot s)}$. Figure 1 displays the isolines of some selected values of the fluidization velocity q^* calculated from (27). In the numerical simulations, we successively apply the bulk flow velocities

$$q(t) = \begin{cases} 0\,\mathrm{m/s} & \text{for } t \in T_1\,, \\ 2.0 \times 10^{-5}\,\mathrm{m/s} & \text{for } t \in T_2\,, \\ 4.0 \times 10^{-5}\,\mathrm{m/s} & \text{for } t \in T_3\,, \\ 6.0 \times 10^{-5}\,\mathrm{m/s} & \text{for } t \in T_4\,, \\ 8.0 \times 10^{-5}\,\mathrm{m/s} & \text{for } t \in T_5\,, \end{cases} \tag{29}$$

where $T_j := [j-1, j) \times 10\,000\,\mathrm{s}$, $j = 1, \ldots, 5$. The values of q for T_2 to T_5 are included in Fig. 1. The intersection of the corresponding iso-lines of q with the straight line representing (26) yields the mixed states $\Phi^i = (\phi_1^{*i}, \phi_2^{*i})^{\mathrm{T}}$ given by

$$\Phi^2 = (0.417, 0.166)^{\mathrm{T}}\,,$$
$$\Phi^3 = (0.288, 0.209)^{\mathrm{T}}\,,$$
$$\Phi^4 = (0.201, 0.238)^{\mathrm{T}}\,,$$
$$\Phi^5 = (0.132, 0.261)^{\mathrm{T}}\,,$$

which are also plotted in Fig. 1. In the transient simulation, we expect that these states will be attained automatically. Besides, one could also prescribe, for example, a mixed state with $\phi_1^* = \phi_2^*$. The proper intersection leads to $\Phi^1 =$

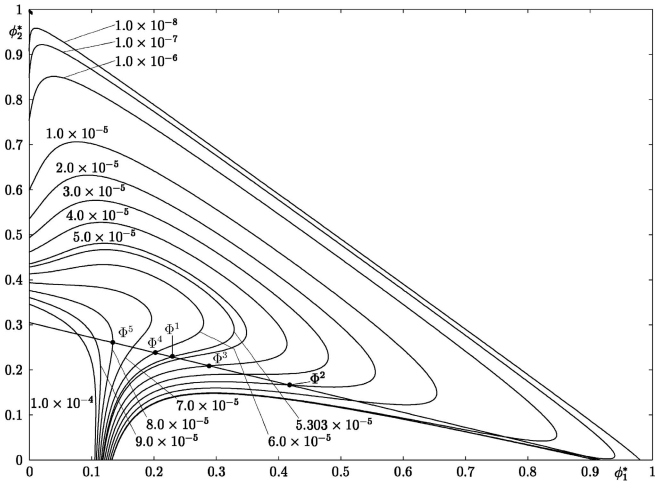

Fig. 1. Completely mixed states Φ^1 to Φ^5 obtained by intersecting curves $q = q(\phi_1, \phi_2) = \text{const}$ with the line representing (26)

$(0.2292, 0.2292)^{\mathrm{T}}$, and we read off from Fig. 1 that $q^* = 5.303 \times 10^{-5}$ is the appropriate fluidization velocity. However, this state is not used in the numerical simulations.

4 Numerical method

In this section we slightly extend the Kurganov-Tadmor central difference scheme as outlined in [1, 4, 14] to the solution of (21) by adding an upwind term for the convective flux $q\Phi$.

To approximate the solution Φ, we introduce a staggered mesh in the (x, t)-plane, where the spatial grid points are denoted by $x_j := j\Delta x$, $j = 0, 1/2, 1, \ldots, \mathcal{J} - 1, \mathcal{J} - 1/2, \mathcal{J}$ and the time levels by $t_n := n\Delta t, \quad n = 0, \ldots, \mathcal{N}$ where $\mathcal{J}$ and $\mathcal{N}$ are integers chosen such that $\mathcal{J}\Delta x = L$ and $\mathcal{N}\Delta t = T$. We denote the length of the space and time steps by Δx and Δt, respectively, and their ratio by $\lambda := \Delta t/\Delta x$.

For details of the computation of the numerical flux $\mathcal{F}_j$, $j = 0, 1/2, \ldots, \mathcal{J}$ used here, we refer to [1, 4]. Given a numerical flux function and defining the discrete values $q^n_{j+1/2} \equiv q$, $j = 0, \ldots, \mathcal{J} - 1$, $n = 0, \ldots, \mathcal{N}$, a scheme for (21) can be written as

$$\bar{\Phi}^{n+1}_j = \bar{\Phi}^n_j - \lambda\big(\mathcal{F}_{j+1/2} - \mathcal{F}_{j-1/2}\big) - \lambda\big(q^n_{j+1/2}\bar{\Phi}^n_{j+1/2} - q^n_{j-1/2}\bar{\Phi}^n_{j-1/2}\big) \tag{30}$$

in the interior ($j = 1, 2, \ldots, \mathcal{J} - 2$) and

$$\bar{\Phi}^{n+1}_0 = \bar{\Phi}^n_0 - \lambda\big(\mathcal{F}_{1/2} + q^n_{1/2}\bar{\Phi}^n_{1/2}\big)$$

on the lower boundary as well as

$$\bar{\Phi}^{n+1}_{\mathcal{J}-1/2} = \bar{\Phi}^n_{\mathcal{J}-1/2} + \lambda\big(\mathcal{F}_{\mathcal{J}-1/2} + q^n_{\mathcal{J}-1/2}\bar{\Phi}^n_{\mathcal{J}-1/2}\big)$$

on the upper boundary.

The extension of the CFL stability condition for the explicit KT scheme stated in [14] for scalar equations to the present case of a hyperbolic system reads

$$\frac{\Delta t}{\Delta z} \max_{\mathcal{D}_{\phi_{\max}}} \varrho\big(\mathcal{J}_{\tilde{f}}(\Phi)\big) \le \frac{1}{4}, \tag{31}$$

where $\tilde{\boldsymbol{f}}(\Phi) := \boldsymbol{f}(\Phi) + q\Phi$. It is emphasized that we view (31) as a *necessary* condition for the present explicit KT scheme to produce a physically relevant numerical result, and that no rigorous convergence result is associated with (31). For that matter, an existence and uniqueness theory for the system (21) is lacking.

5 Numerical simulations

For the simulations, we use a settling column of height $H = 1.0\,\mathrm{m}$ and cut the hindered settling function at $\phi_{\max} = 0.58$. The initial concentration is given by $\Phi^0 = (0.15, 0.15)^{\mathrm{T}}$. Following the discussion of [5, Sect. 5.1], the relatively low maximum concentration was chosen to ensure that the model equations are hyperbolic.

The steady-state condition (26) now reads $\phi_2 = 0.31 - 0.33\phi_1$ and the mixing condition (28) is $\phi_2 = \phi_1$. Further, a grid with $\mathcal{J} = 480$ cells and $\lambda = 50$ is chosen.

The simulations shown in Figs. 2 and 3 were run without fluidization ($q = 0$). The left plot in Fig. 2 illustrates that, at a small total solids concentration, the larger species settles faster. At the same time, the smaller species forms a zone above the upper interface of the larger species where their concentration is higher than the initial. This phenomenon was first explained by Smith [21] and is sometimes called the *Smith effect.*

The middle plot of Fig. 2 shows that, after the larger particles have completely settled, the smaller particles do not just simply settle onto the existing sediment, as one might expect, building a layer consisting of just the smaller particles. Rather, the fairly equally partitioned solids concentration at the lower boundary of the 'nose' (say, $\phi_1 \approx \phi_2 \approx \phi/2 > 0.25$) causes the local velocity of the larger species to change sign (since $\bar{\varrho}_1 - \bar{\boldsymbol{\varrho}}^{\mathrm{T}}\Phi \approx \bar{\varrho}_1 - (\bar{\varrho}_1 + \bar{\varrho}_2)\phi/2 < 0$) so that the larger particles at the boundary move upwards making space for the smaller particles and thus the nose settles down.

Finally, the right plot of Fig. 2 illustrates that the settling 'nose' (consisting of smaller species) causes the re-formation of a new sediment bed which grows from the bottom. This consists entirely of the smaller particles. After the settling nose has completely settled and displaced larger particles, a mixed bed forms above the sediment where the dominance of the smaller species decreases with height. Fig. 3 provides a more extensive (but less accurate) illustration of the initial batch settling ($q = 0$) phase of the simulation.

Now we deal with the fluidization process where the fluidizing velocity $q(t)$ is given by (29). In view of Fig. 4, the assumption that the total fluidized bed can be divided into two

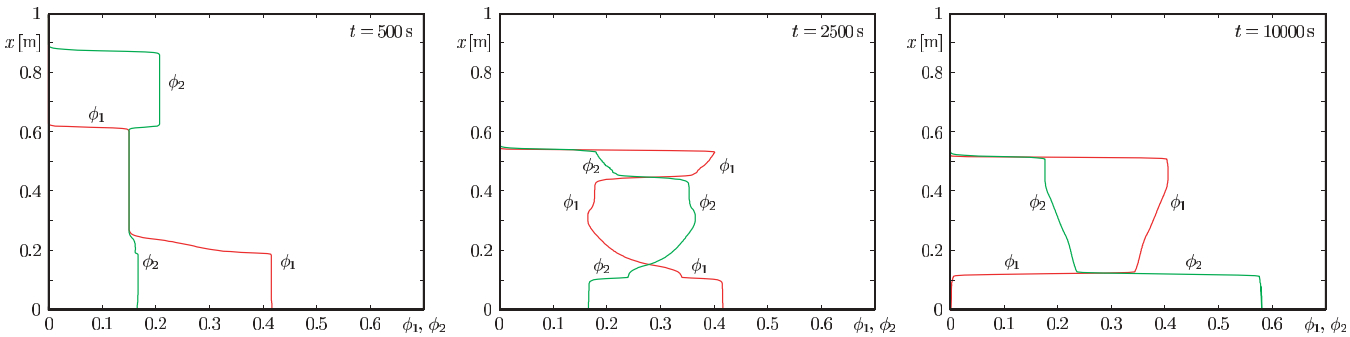

Fig. 2. Numerical simulation of batch sedimentation ($q = 0$) of an initially homogeneous bidisperse suspension: profiles of the concentrations ϕ_1 (*red*) and ϕ_2 (*green*) of the larger and smaller particles at the indicated times

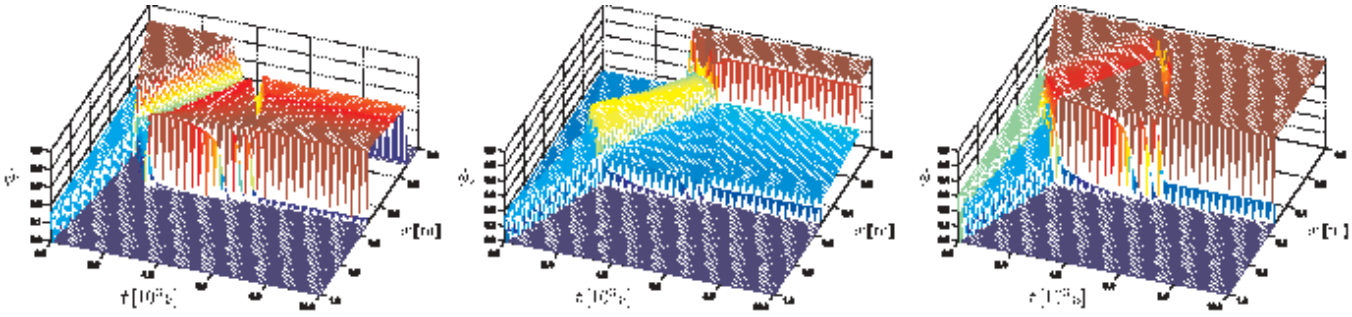

Fig. 3. Numerical simulation of batch sedimentation ($q = 0$) of an initially homogeneous bidisperse suspension: concentrations ϕ_1 and ϕ_2 of the larger and smaller particles (*left and middle*) and cumulative solids concentration ϕ (*right*)

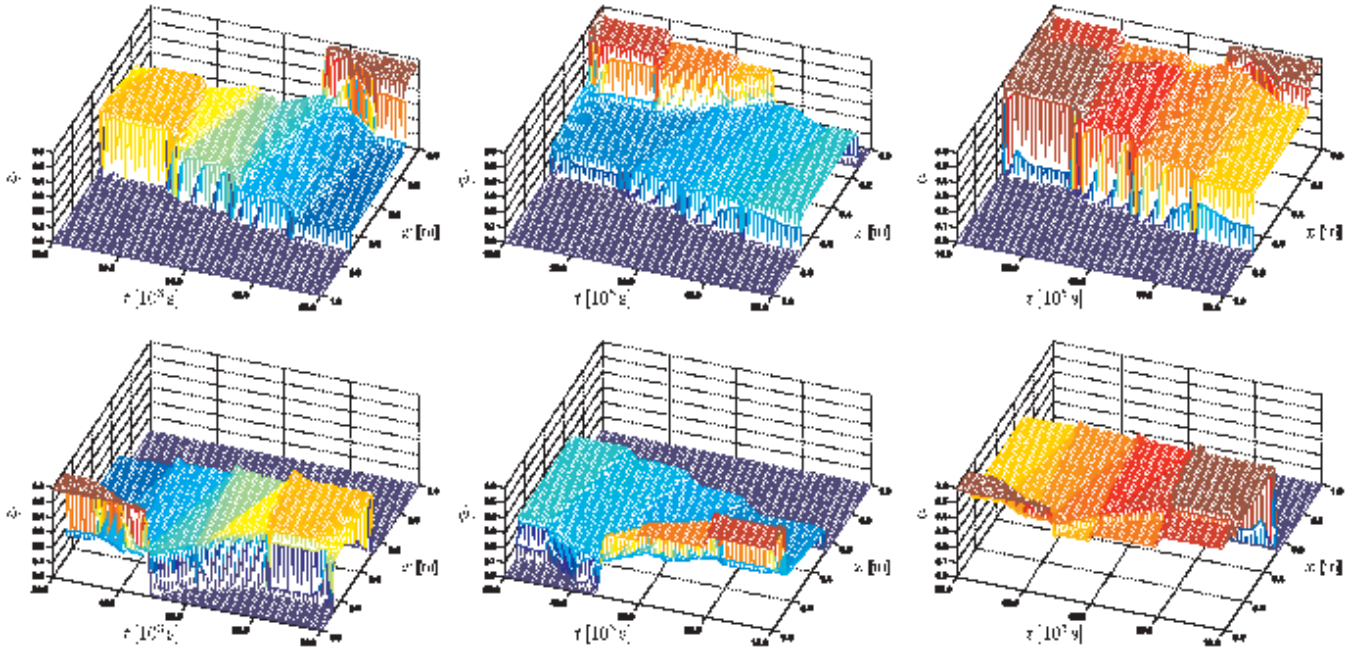

Fig. 4. Continuation of the numerical experiment of Fig. 3: simulation of bed inversion with a succesively increased fluidization velocity $q = q(t)$. *Top row*: views 'from above' of the concentrations ϕ_1 and ϕ_2 of the larger and smaller particles (*left and middle*) and of the cumulative solids concentration ϕ (*right*). *Bottom row*: the same results viewed 'from below'

layers with respective constant solids concentrations can be affirmed. However, in our example, in the upper layer there is a mixture consisting of both species with neither having a negligible concentration. Thus, it is evident that a serial model [10, 11] which assumes each layer to be monodisperse is a rather coarse simplification.

We refer to the two distinguishable layers as *upper* and *lower*. After each increase of the fluidizing velocity, two fronts in the upper level can be observed (Fig. 4). The first front, where only the larger species is involved, starts at the interface of the lower layer, travels relatively fast upwards and ends with a 'pike', which sharply raises the bed of the larger particles. The concentration of the smaller species in the upper layer does not change while the first front is traveling upwards. The second front starts in the top of the pike, moves more slowly than the first, and finally meets the interface of the meanwhile increased lower layer. The second front causes another decrease in concentration of the larger species and, at the same time, an increase of the smaller species in the upper layer. At the same time as the second front in the upper layer travels down, there travels a front at the interface between the upper and the lower layer causing a change of the lower bed height. In the lower layer, the bed in the phase of the smaller particles is reduced or, when there is no more bed to reduce, the void space is enlarged. In the phase of the larger particles, the void space in the lower layer is reduced or, after inversion, the bed is increased.

In Fig. 5, the Lagrangian paths of the solids concentrations are computed with respect to the 5%, 10%, 20%, ..., 90%, 95% quantile of the respective solids concentration. The initial settling is not shown completely because of the coarse visual grid. Bed expansion is reflected by the steep rising of the paths after increasing q. Bed inversion can be recognized by the decreasing of the paths of the larger species. When the fluidizing velocity is increased from $q < q^{\mathrm{mix}}$ to $q > q^{\mathrm{mix}}$, bed inversion can be observed. Comparing the Lagrangian paths, one can remark the dramatic change in the particle order. The smaller spheres rise all over the container so that the larger particles may sink into lower regions. When the fluidizing velocity has exceeded the mixing velocity, after each increase

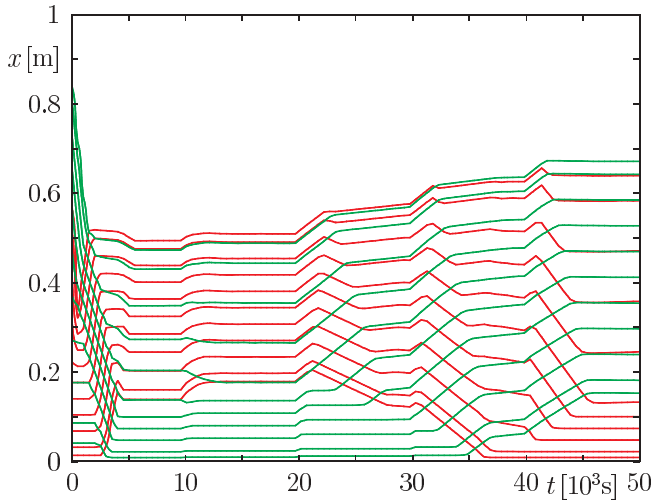

Fig. 5. Lagrangian paths of the solids concentrations with respect to the 5%, 10%,20%,...,90%, 95% quantiles of larger species (*red*) and the smaller species (*green*)

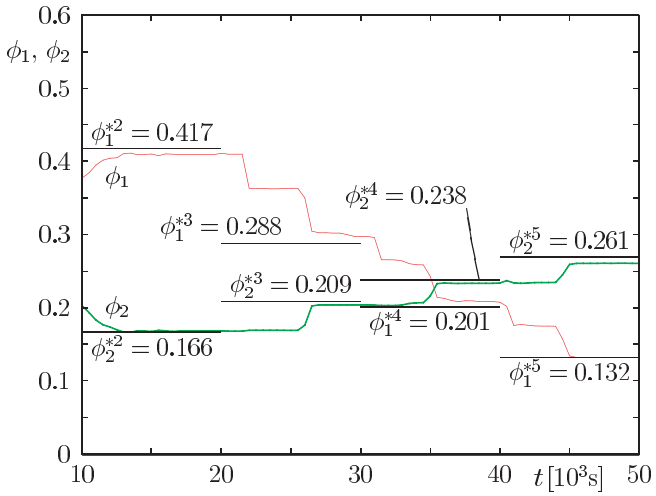

Fig. 6. Simulated concentrations ϕ_1 of the larger species (*red*) and ϕ_2 of the smaller species (*green*) taken at height $x = 0.30$ m. The plot also shows the exact concentrations of the mixed states

in q, the paths of the smaller species rise upwards while the paths of the larger species first rise and then fall until the bed is reached.

In Fig. 6, the concentration of both species at the fixed height $x = 0.30\,\mathrm{m}$ is plotted as a function of time. Since, during the entire simulation time, this specific height x lies inside the upper mixed layer (where both species are present), whereas the lower layer is always depleted by one species, the simulated concentrations approximate the values calculated in Fig. 1. This is reasonable since, for bidisperse suspensions, the mixing state is unique for a given fluidization velocity.

6 Discussion

In the present paper, we have applied the MLB model to fluidization by viewing it as a conservation law. The simulation, with a high-resolution scheme, demonstrates the qualitative concordance with experiments with the only restriction that, from experiments, one would expect a stronger bed expansion. The fact that, in the simulations, the bed does not expand as significantly indicates that the chosen MLB model does not explicitly take this phenomenon into account. Nevertheless, it is shown that the most obvious observed phenomenon in fluidization, bed inversion, is reflected by the model.

Our treatment is restricted to the bidisperse case ($N = 2$) since the focus is to demonstrate that fluidization forms an interesting application of (not necessarily hyperbolic) systems of first-order nonlinear partial differential equations. Whenever the compatibility condition is satisfied, it is expected that a stationary N-disperse suspension with $\delta_1 > \delta_2 > \cdots > \delta_N$ and $\bar{\varrho}_1 < \bar{\varrho}_2 < \cdots < \bar{\varrho}_N$ is divided into N regions with respective constant concentrations, one consisting of N different species, a second with $N-1$ species and so on. Complete mixing is reached if for given q the initial condition, Φ^0 has been chosen appropriately. This generalizes the observation that, for $N = 2$ and for arbitrary initial condition, there is one region that is completely mixed and a second region that contains the excess of the other species.

To find the steady states in the general case ($N \geq 2$), one could also start with an alternative interpretation of (23) as special case of the Rankine-Hugoniot condition

$$\boldsymbol{F}\left(\Phi^k\right) - \boldsymbol{F}\left(\Phi^{k-1}\right) = s_k\left(\Phi^k - \Phi^{k-1}\right), \quad k = 2, \ldots, N,$$

where $\boldsymbol{F}\left(\Phi^k\right) := \left(F_1\left(\phi_1^k\right), \ldots, F_N\left(\phi_N^k\right)\right)^{\mathrm{T}}$. If the stationary state is reflected by $s_k = 0, k = 2, \ldots, N$ and $\Phi^1 := (0, \ldots, 0)^{\mathrm{T}}$ denotes the concentration in the clear-liquid zone, then the solutions $\Phi^2, \ldots, \Phi^{N+1}$ of

$$\boldsymbol{F}\left(\Phi^k\right) = 0, \quad k = 2, \ldots, N+1 \tag{32}$$

correspond to the concentrations of the suspension in the N layers.

Acknowledgements. This work has been supported by the Applied Mathematics for Industrial Flow Problems (AMIF) programme of the European Science Foundation (ESF) and by the Sonderforschungsbereich 404 at the University of Stuttgart.

References

1. Berres, S., Bürger, R., Karlsen, K.H., Tory, E.M.: Strongly degenerate parabolic-hyperbolic systems modeling polydisperse sedimentation with compression. SIAM J. Appl. Math. 64, 41–80 (2003)
2. Bürger, R., Concha, F., Fjelde, K.-K., Karlsen, K.H.: Numerical simulation of the settling of polydisperse suspensions of spheres. Powder Technol. 113, 30–54 (2000)
3. Bürger, R., Evje, S., Karlsen, K.H.: On strongly degenerate convection-diffusion problems modeling sedimentation-consolidation processes. J. Math. Anal. Appl. 247, 517–556 (2000)
4. Bürger, R., Fjelde, K.-K., Höfler, K., Karlsen, K.H.: Central difference solutions of the kinematic model of settling of polydisperse suspensions and three-dimensional particle-scale simulations. J. Eng. Math. 41, 167–187 (2001)
5. Bürger, R., Karlsen, K.H., Tory, E.M., Wendland, W.L.: Model equations and instability regions for the sedimentation of polydisperse suspensions of spheres. Z. Angew. Math. Mech. 82, 699–722 (2002)
6. Bürger, R., Wendland, W.L.: Existence, uniqueness and stability of generalized solutions of an initial-boundary value problem for a degenerating quasilinear parabolic equation. J. Math. Anal. Appl. 218, 207–239 (1998)

7. Bürger, R., Wendland, W.L., Concha, F.: Model equations for gravitational sedimentation-consolidation processes. Z. Angew. Math. Mech. 80, 79–92 (2000)
8. Bustos, M.C., Concha, F., Bürger, R., Tory, E.M.: Sedimentation and Thickening: Phenomenological Foundation and Mathematical Theory. Dordrecht: Kluwer Acad. Publ. 1999
9. Davis, R.H., Gecol, H.: Hindered settling function with no empirical parameters for polydisperse suspensions. AIChE J. 40, 570–575 (1994)
10. Epstein, N., LeClair, B.P., Pruden, B.B.: Liquid fluidization of binary particle mixtures – I. Overall bed expansion. Chem. Eng. Sci. 36, 1803–1809 (1981)
11. Epstein, N., LeClair, B.P.: Liquid fluidization of binary particle mixtures – II. Bed inversion. Chem. Eng. Sci. 40, 1517–1526 (1985)
12. Galvin, K.P., Pratten, S., Nguyen Tran Lam, G.: A generalized empirical description for particle slip velocities in liquid fluidized beds. Chem. Eng. Sci. 54, 1045–1052 (1999)
13. Gibilaro, L.G., Di Felice, R., Waldram, S.P., Foscolo, P.U.: A predictive model for the equilibrium composition and inversion of binary-solid liquid fluidized beds. Chem. Eng. Sci. 41, 379–387 (1986)
14. Kurganov, A., Tadmor, E.: New high resolution central schemes for nonlinear conservation laws and convection-diffusion equations. J. Comp. Phys. 160, 241–282 (2000)
15. Lockett, M.J., Bassoon, K.S.: Sedimentation of binary particle mixtures. Powder Technol. 24, 1–7 (1979)
16. Masliyah, J.H.: Hindered settling in a multiple-species particle system. Chem. Eng. Sci. 34, 1166–1168 (1979)
17. Moritomi, H., Iwase, T., Chiba, T.: A comprehensive interpretation of solid layer inversion in liquid fluidised beds. Chem. Eng. Sci. 37, 1751–1757 (1982)
18. Moritomi, H., Yamagishi, T., Chiba, T.: Prediction of complete mixing of liquid-fluidized binary solid particles. Chem. Eng. Sci. 41, 297–305 (1986)
19. Nessyahu, H., Tadmor, E.: Non-oscillatory central differencing for hyperbolic conservation laws. J. Comp. Phys. 87, 408–463 (1990)
20. Patwardhan, V.S., Tien, C.: Sedimentation and liquid fluidization of solid particles of different sizes and densities. Chem. Eng. Sci. 40, 1051–1060 (1985)
21. Smith, T.N.: The sedimentation of particles having a dispersion of sizes. Trans. Instn. Chem. Engrs. 44, T152–T157 (1966)
22. Weiland, R.H., Fessas, Y.P., Ramarao, B.V.: On instabilities arising during sedimentation of two-component mixtures of solids. J. Fluid Mech. 142, 383–389 (1984)
23. Xue, B., Sun, Y.: Modeling of sedimentation of polydisperse spherical beads with a broad size distribution. Chem. Eng. Sci. 58, 1531–1543 (2003)